BEILSTEIN JOURNAL OF ORGANIC CHEMISTRY

Sulfated prism[6]arene binds one guest internally and one guest externally

Emmanuel A. Bazan-Bergamino[1], Steven Ayoub[2], David L. Mobley[*2] and Lyle Isaacs[*1]

Full Research Paper

Open Access

Address:
[1]Department of Chemistry and Biochemistry, University of Maryland, College Park, Maryland 20742, United States and [2]Department of Pharmaceutical Sciences and Department of Chemistry, University of California, Irvine, CA 92697, United States

Email:
David L. Mobley[*] - dmobley@uci.edu; Lyle Isaacs[*] - LIsaacs@umd.edu

* Corresponding author

Keywords:
host–guest systems; macrocyclic arene; prismarene; ternary complex

Beilstein J. Org. Chem. **2026,** *22,* 1635–1648.
https://doi.org/10.3762/bjoc.22.132

Received: 27 August 2026
Accepted: 26 October 2026
Published: 11 November 2026

This article is part of the thematic issue "Physical organic chemistry of new materials".

Guest Editor: J. D. Tovar

© 2026 Bazan-Bergamino et al.; licensee Beilstein-Institut.
License and terms: see end of document.

Abstract

We report the synthesis of sulfated prism[6]arene (Pr[6]AS) by reaction of $(HO)_{12}$Pr[6] with SO_3·pyridine in 35% yield. Pr[6]AS has very good solubility in water (>30 mM) and does not undergo self-association according to ^{1}H NMR dilution experiments. Qualitative ^{1}H NMR investigations show that guest resonances shift dramatically upfield and become significantly broadened upon complexation with Pr[6]AS. Isothermal titration calorimetry (ITC) experiments show that Pr[6]AS forms ternary complexes (Pr[6]AS·guest$_2$) with hydrophobic ammonium ions in phosphate buffered saline with β-values ($K_{a1} \times K_{a2}$) values up to 6.84×10^{13} M^{-2}. Molecular dynamics simulations show that Pr[6]AS firmly binds one guest (**6q**, Me_4Bipip) within its cavity and a second guest (**6q**, Me_4Bipip) on the convex region of Pr[6]AS in close proximity to the externally directed sulfate substituents. Uncomplexed Pr[6]AS holds 7.6 ± 1.9 H_2O and one Na^+ ion within its cavity. Formation of the 1:1 and 1:2 Pr[6]AS–**6q** complexes results in expulsion of the Na^+ ion and approximately five of the solvating H_2O molecules. Intriguingly, the combination of larger naphthalene walls and sulfate ionic groups that are conformationally restricted creates a secondary guest binding site on the exterior of Pr[6]AS which suggests a route toward the design of high molecularity complexes.

Introduction

Modern supramolecular chemistry relies on the ready availability of building blocks that can be used to create functional systems like biological imaging agents, drug delivery systems, separations materials, chemical sensors, and stimuli-responsive materials [1-6]. Macrocycles constitute an important class of supramolecular building blocks that most commonly form binary macrocycle·guest complexes. Some of the most popular macrocyclic host families include cyclodextrins, crown ethers, cavitands, calixarenes, cyclophanes, metal-organic cages, cucurbiturils, and most recently pillararenes (Figure 1a) [7-15]. Macrocycles that form binary complexes with ultrahigh binding affinity (e.g., CB[*n*]) and high selectivity are particularly prized

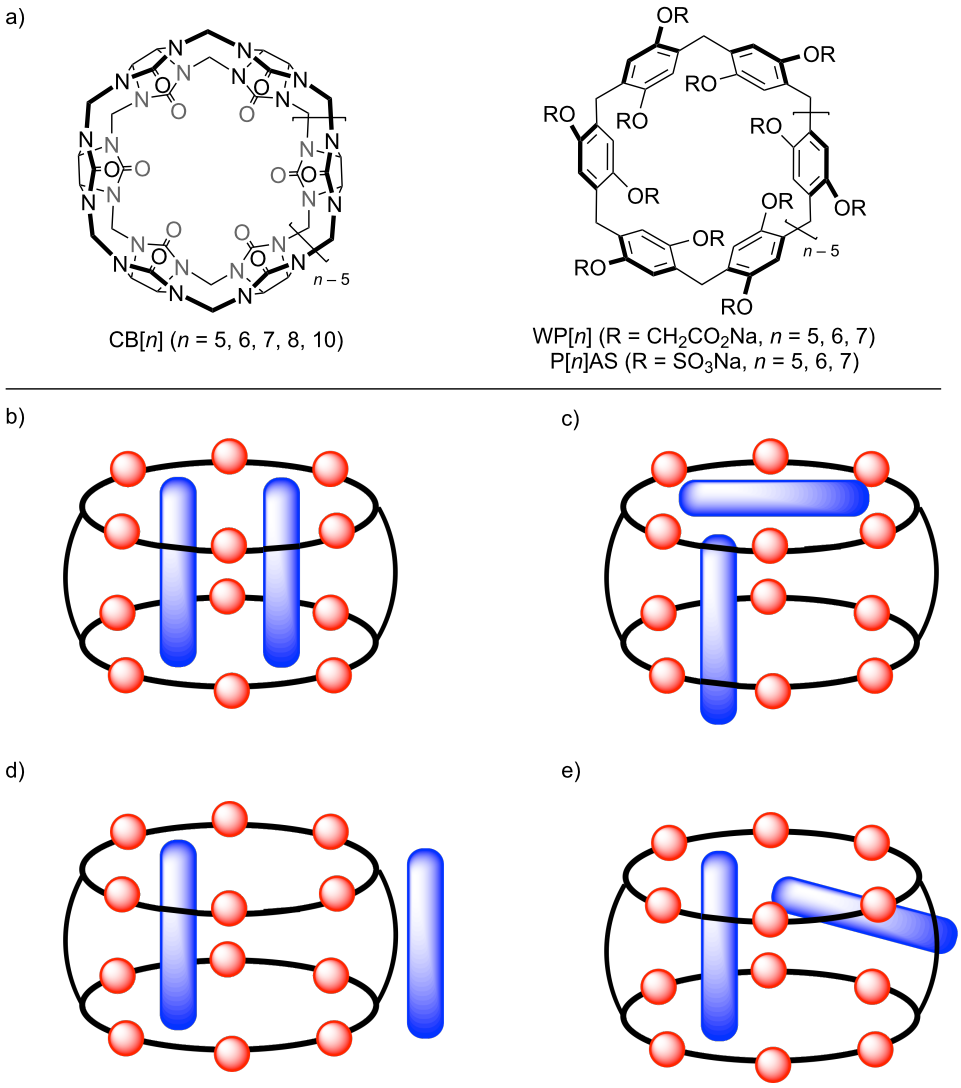


Figure 1: a) Structures of selected water-soluble host systems. Depictions of different geometries of host·(guest)$_2$ complexes: b) in-in, c) in-portal, d) in-out$_{axial}$, and e) in-out$_{equatorial}$.

for non-covalent latching, surface immobilization, and even *in vivo* sequestration [16-18]. Consequently, a subset of supramolecular chemists seek to understand the design principles governing ultrahigh affinity complexation in water [19,20]. Conversely, macrocycles that display moderate affinity and selectivity (e.g., cyclodextrins) are more appropriate as solubilizing excipients for insoluble drugs and as components of sensing arrays [21]. Within a homologous family of macrocycles, the larger ring sizes are sometimes capable or forming not only binary, but also ternary or even quaternary complexes [22-24]. For example, the ability of CB[8] to form homo-ternary and hetero-ternary complexes has been used to construct self-assembled materials, stimuli-reponsive molecular switches, and promote protein dimerization [25-27]. Other capacious cyclindrical hosts have been used to promote reactions and interactions between encapsulated guests [11,28-32]. For example, Fujita's earliest tetrahedral metal-organic cage cooperatively binds four equivalents of adamantanecarboxylic acid and later tubular variants even template the assembly of tetramolecular donor–acceptor π-stacks for electron transport [23,33,34]. In the above-mentioned systems, the two or more guests bind inside the cavity of the host (Figure 1b). Other hosts, particularly water-soluble macrocycles featuring large aromatic walls form ternary complexes where one guest is bound inside the macrocyclic cavity and a second guest binds to the outer π-surface of the host (Figure 1d). For example, Badjić's molecular bowls form ternary complexes with methotrexate and phenethylamines [35,36].

Within this context, our group sought to use our understanding of the ultrahigh binding affinity of cucurbiturils (e.g., electrostatically negative portals; release of high-energy waters) to improve the binding affinity of water-soluble pillararenes (WP[*n*], Figure 1a) [37]. Accordingly, we removed the hydrophobic CH_2-linker to prevent self-inclusion and swapped CO_2Na for OSO_3Na to ensure complete deprotonation at all pH values to create pillar[*n*]MaxQ (P[*n*]AS) [38]. P[*n*]AS display ultrahigh binding affinity in water and bind preferentially to quaternary ammonium ions. We have investigated the origins of the ultrahigh binding affinity of P[*n*]AS and used P[6]AS as an *in vivo* reversal agent for drugs of abuse and neuromuscular blockers [39-44]. Other researchers have applied P[*n*]AS directly along with related sulfated macrocyclic arenes in a variety of applications [45-49].

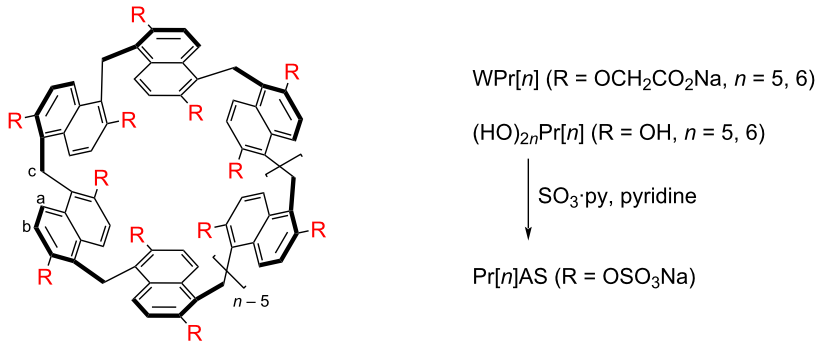
In 2020, the work of Gaeta on organic soluble prismarenes based on 2,6-dialkoxynaphthalene monomers caught our eye [50] as a way to increase macrocycle depth and volume and perhaps enhance the π–π and hydrophobic contributions to aqueous binding free energy. Thereafter, Gaeta's group published the synthesis of water-soluble prism[*n*]arene (Scheme 1, WPr[*n*], *n* = 5, 6) and our group published a direct cyclization route toward WPr[5] and demonstrated its high binding affinity toward hydrophobic dications [51,52]. Naturally, we sought to apply our sulfate trick to the prismarene scaffold and recently reported the synthesis of Pr[5]AS and showed that it binds significantly more strongly than WPr[5] toward a common guest [53]. Very recently, Gaeta reported the synthesis of Pr[6]AS from $(HO)_{12}$Pr[6] and showed that it is a very effective host for the environmental pollutants methylene blue and rhodamine B [54]. Herein, we report our synthesis of Pr[6]AS and its ability to form ternary Pr[6]AS·$(guest)_2$ complexes with hydrophobic diammonium ions.

Results and Discussion

This Results and Discussion section is organized as follows. First, we describe the synthesis and characterization of Pr[6]AS along with the determination of its inherent aqueous solubility and its low propensity for self-association by ^{1}H NMR dilution experiments. Next, we study the binding of Pr[6]AS with a panel of hydrophobic guests by ^{1}H NMR spectroscopy at different Pr[6]AS:guest ratios. Thereafter, we present the results of isothermal titration calorimetry (ITC) experiments that establish the formation of ternary Pr[6]AS·$(guest)_2$ complexes. Molecular dynamics simulations were then used to study Pr[6]AS alone and in combination with one or two equivalents of guest. Finally, we offer some conclusions.

Design, synthesis, and characterization of Pr[6]AS

As described above, swapping of CH_2CO_2H solubilizing arms for strictly hydrophilic and ionic solubilizing sulfate groups effectively enhances binding affinity of Pr[5]AS relative to WPr[5] and of P[6]AS relative to WP[6] [38,53]. Given that WPr[6] displays only modest affinity toward neutral and cationic guests in water (log K_a up to 3.5) [51,55,56], we saw an opportunity to greatly enhance binding affinity via host sulfation. Accordingly, we synthesized $(HO)_{12}$Pr[6] according to the procedure of Gaeta [57]. Next, we reacted $(HO)_{12}$Pr[6] with 30 equivalents of pyridine·sulfur trioxide complex in pyridine at 60 °C for 36 hours to give Pr[6]AS as a crude solid. Pure Pr[6]AS was obtained in 35% yield after basification with $NaHCO_3$ followed by reprecipitation from water using acetone (Supporting Information Information File 1). The water solubility of Pr[6]AS was determined as ≥30 mM by standard gravimetric and volumetric methods. The ^{1}H NMR spectrum recorded for Pr[6]AS (Figure 2a) displays a pair of doublets in the aromatic region of the spectrum and a singlet for the bridging CH_2-groups; the spectrum is equivalent to that reported by



Scheme 1: a) Structures of various prism[*n*]arenes (*n* = 5, 6) and the synthesis of Pr[6]AS. Conditions: a) pyridine·SO_3 (30 equiv), pyridine, 60 °C, 1.5 days, 35%.

Gaeta [54]. This pattern of resonances is consistent with Pr[6]AS adopting a time-averaged D_6-symmetric conformation. It is known that prism[6]arenes are planar chiral and can adopt eight different conformations [58] which may explain the small resonances seen in the baseline of Figure 1a. The ^{13}C NMR spectrum recorded for Pr[6]AS (Figure 2b) shows five aromatic resonances for the symmetry-equivalent naphthalene walls and one resonance for the bridging CH_2 groups at 20.4 ppm as expected for time-averaged D_6-symmetry. The electrospray ionization (ESI) mass spectrum recorded in the negative ion mode for Pr[6]AS (Supporting Information File 1, Figure S3) displays a prominent ion at m/z = 718.89 which can be assigned as $[Pr[6]AS - 8SO_3Na + 6H\}^{2-}$ (calcd for $C_{66}H_{42}O_{24}S_4Na_4^{2-}$, 719.03) and less intense ions at m/z = 668.04 and 789.90 which correspond to $[Pr[6]AS - 9SO_3Na + 7H\}^{2-}$ and $[Pr[6]AS - 8SO_3Na + 6H + Na_2SO_4\}^{2-}$, respectively.

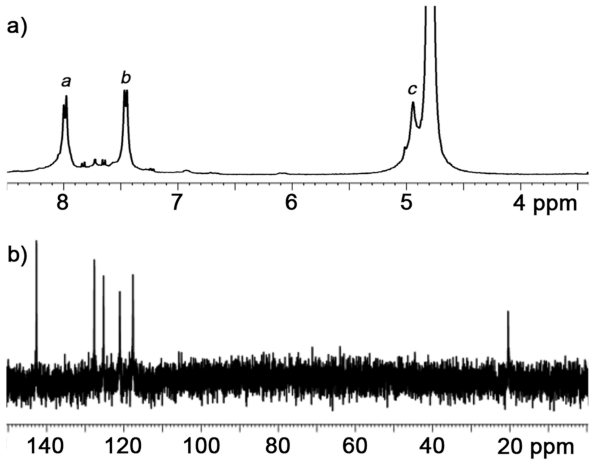


Figure 2: a) ^1H NMR spectrum (600 MHz, D_2O, 298 K) recorded for Pr[6]AS, and b) ^{13}C NMR spectrum recorded (150 MHz, D_2O, 298 K) for Pr[6]AS.

After having firmly established the structure of Pr[6]AS spectroscopically, we set out to determine whether Pr[6]AS undergoes self-association in aqueous solution that might impinge upon the measurement of host·guest-binding thermodynamics. For this purpose, we performed ^1H NMR dilution experiments and monitored the chemical shifts as a function of [Pr[6]AS] from 50 μM to 5 mM (Supporting Information File 1, Figures S5 and S6). We observed only very small ($\Delta\delta \leq 0.03$ ppm) changes in chemical shifts which indicates that Pr[6]AS does not undergo significant self-association in water. We also performed variable-temperature ^1H NMR experiments (Supporting Information File 1, Figure S4) for Pr[6]AS over the 293–343 K temperature range, but did not observe sharpening of the spectrum relative to Figure 2a suggesting that Pr[6]AS dynamics are slow on the chemical shift timescale.

Qualitative investigation of the molecular recognition properties of Pr[6]AS by ^1H NMR spectroscopy

Next, we investigated the molecular recognition properties of Pr[6]AS toward a panel of guests (Figure 3) by ^1H NMR spectroscopy at different Pr[6]AS:guest molar ratios. The guest panel was selected to include guests of gradually increasing cross-sectional area and hydrophobicity as well as include primary and quaternary ammonium ions. Figure 4a and 4f show the ^1H NMR spectra recorded for Pr[6]AS and **6q** (Me_4Bipip) separately. Figure 4b–e show the ^1H NMR spectra recorded at 1:1, 1:2, 1:3, and 1:4 host:guest molar ratios. At a 1:1 Pr[6]AS:**6q** molar ratio (Figure 4b), the guest resonances broaden dramatically and shift significantly upfield upon complexation with the following Δδ values for H_o (−2.28), H_p (−2.36), and H_q (−2.58) located in the center of **6q**. The resonances for H_k–H_n located nearer the ends of **6q** undergo smaller changes in chemical shift (H_k: −0.42; H_l: −0.92; H_m: −1.08; H_n: −1.39). This pattern of resonances indicates that on a time-averaged basis the center of the **6q** guest is located within the anisotropic magnetic shielding region of one or more of the naphthalene walls of Pr[6]AS. Related ^1H NMR stack plots for the other guests are given in Supporting Information File 1 (Figures S7–S19). Table 1 presents the Δδ values observed for each guest at a 1:1 Pr[6]AS:guest ratio. Similar Δδ patterns are observed for other guests which indicates they adopt related geometries with the central hydrophobic regions of the guest located near the magnetically shielding naphthalene walls and the ammonium groups located closer to the sulfated portals. At higher **6q**:Pr[6]AS ratios (Figure 4c–e) the guest resonances shift gradually back toward the location of free **6q** (Me_4Bipip) which indicates that the kinetics of guest exchange are in the intermediate to fast exchange regime on the chemical shift timescale. However, the magnitude of the backshifting of resonances was less than would be expected for a simple 1:1 complex. For example, the Δδ value for H_q of **6q** at a 1:1 ratio is −2.58 ppm, at a 1:2 ratio is −2.42 ppm, at a 1:3 ratio is −2.37 ppm, and is −1.93 ppm at a 1:4 ratio. For a hypothetical 1:1 mixture of Pr[6]AS·**6q** and **6q** under fast exchange, a 50% reduction in the Δδ value from −2.58 to −1.29 ppm would be expected, but we only see a 6% reduction to −2.42 ppm. Related changes in chemical shifts at 1:2 and 1:4 molar ratios are seen with the other guests. These results suggested that Pr[6]AS is capable of binding at least two guest molecules at the concentration of Pr[6]AS (100 μM) used for ^1H NMR. We also monitored the chemical shift of Pr[6]AS (H_b) upon titration with **2q**, **3q**, **5q**, and **6q** (1, 2, 3, and 4 equiv). A plot of Δδ versus guest concentration (Supporting Information File 1, Figure S20) shows that the change in chemical shift plateaus at an approximate 1:2 Pr[6]AS:guest ratio which provides additional support for a 1:2 binding model.

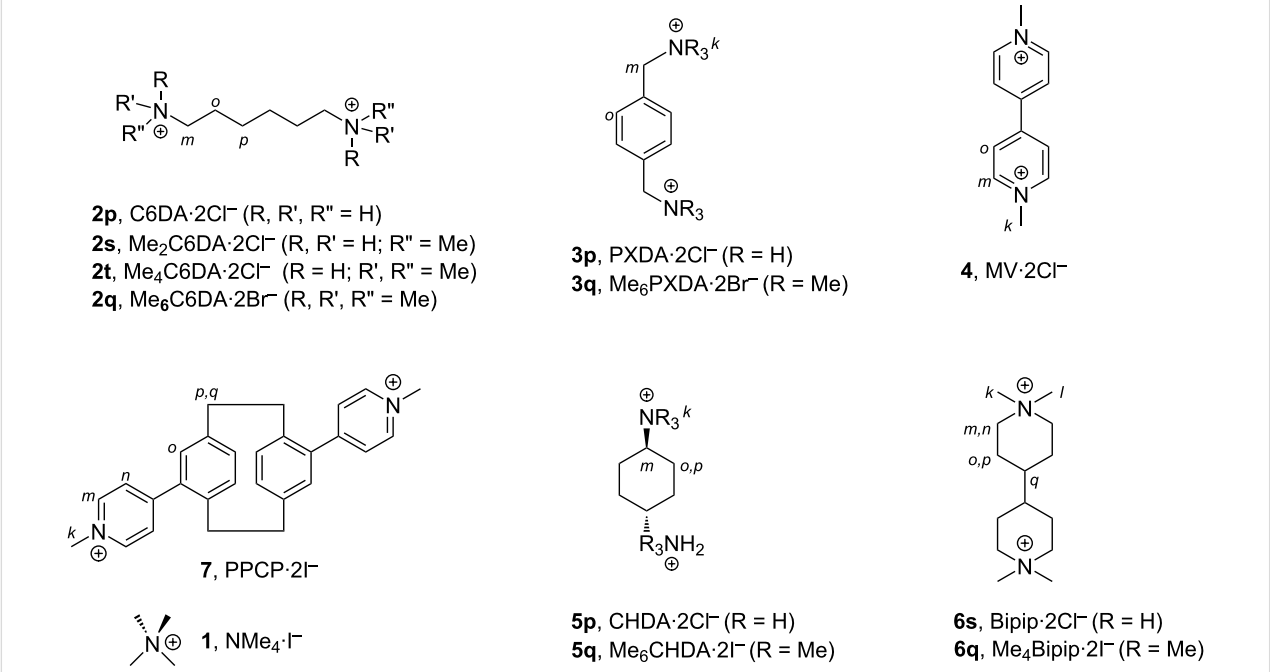


Figure 3: Structures of guests used in this study and proton labelling.

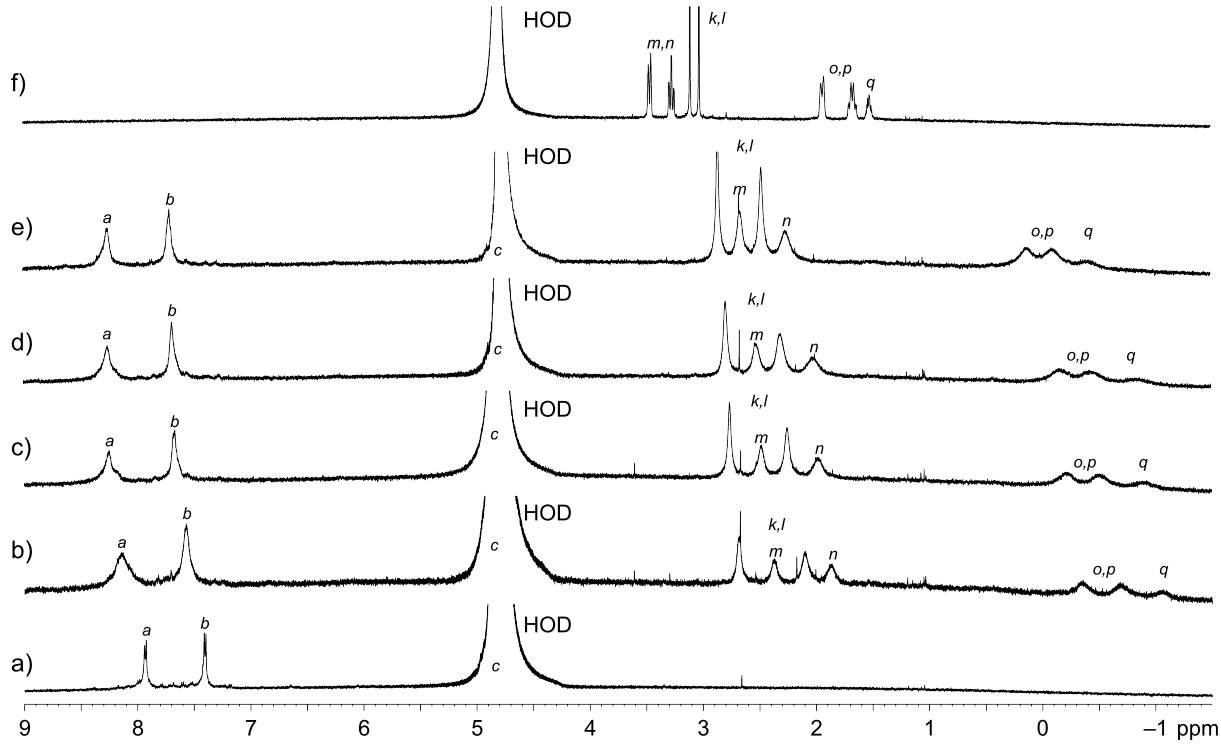


Figure 4: ^{1}H NMR spectra (600 MHz, D_2O, rt) recorded for: a) Pr[6]AS (100 μM), b) a mixture of Pr[6]AS (100 μM) and **6q** (Me_4Bipip) (100 μM), c) a mixture of Pr[6]AS (100 μM) and **6q** (200 μM), d) a mixture of Pr[6]AS (100 μM) and **6q** (300 μM), e) a mixture of Pr[6]AS (100 μM) and **6q** (400 μM), and f) **6q** (400 μM).

Table 1: Complexation-induced changes in chemical shifts (Δδ) for indicated guest resonances at a 1:1 Pr[6]AS:guest molar ratio.

Guest	*k*	*l*	*m*	*n*	*o*	*p*	*q*
1, NMe_4	–0.32	–	–	–	–	–	–
2p, C6DA	–	–	–1.69	–	–1.99	–2.74	–
2s, Me_2C6DA	–0.63	–	–1.89	–	–1.97	–2.72	–
2t, Me_4C6DA	–0.62	–	–1.96	–	–2.17	–2.88	–
2q, Me_6C6DA	–0.64	–	–1.75	–	–2.42	–2.97	–
3p, PXDA	–	–	–1.14	–	–1.42	–	–
3q, Me_6PXDA	–0.85	–	–1.30	–	–2.08	–	–
4, MV	–0.15	–	–0.80	–	–2.65	–	–
5p, CHDA	–	–	–0.72	–	–0.82	–0.77	–
5q, Me_6CHDA	–1.05	–	–1.86	–	–2.21	–2.30	–
6s, Bipip	–	–	–0.92	–1.54	–2.32	–1.77	–2.62
6q, Me_4Bipip	–0.42	–0.92	–1.08	–1.39	–2.28	–2.36	–2.58

Quantitative investigation of the molecular recognition properties of Pr[6]AS by isothermal titration calorimetry

As described above, the upfield shifts in chemical shift upon complexation persist at higher guest:Pr[6]AS stoichiometries which suggested the formation of ternary Pr[6]AS·$guest_2$ and potentially higher molecularity complexes. We expected that Pr[6]AS would form tight complexes with hydrophobic dications and therefore we selected ITC as our analytical method since it is able to easily determine K_a values up to 10^{12} M^{-1} by direct and competitive ITC titrations along with ΔH and stoichiometry (N-value). Figure 5a shows the thermogram recorded when a solution of Pr[6]AS (10 μM) in phosphate-buffered saline (PBS) in the ITC cell was titrated with a PBS solution of **6q** (Me_4Bipip, 200 μM) from the ITC syringe. The peaks in Figure 5a were integrated to obtain the heat evolved per injection and then a plot of ΔH versus molar ratio was created (Figure 5b). The data exhibits a clear inflection point at a molar ratio of ≈2 which indicates the formation of the Pr[6]AS·$\mathbf{6q}_2$ ternary complex. The data in Figure 5b could be fitted equally well to either a single-set-of-sites binding model with $N = 2$ or to a sequential binding with the PEAQ ITC data analysis software. The molecular dynamics simulations reported below show two distinct binding sites and therefore support the application of a sequential binding model. The solid line in Figure 5b represents the best fit of the data to the sequential binding model implemented within the PEAQ data analysis software with $K_{a1} = (1.28 \pm 0.11) \times 10^6$ M^{-1} and $\Delta H_1 = -12.33 \pm 1.15$ kcal mol^{-1} and $K_{a,2} = (6.48 \pm 0.31) \times 10^5$ M^{-1} and $\Delta H_2 = -12.63 \pm 1.42$ kcal mol^{-1} (Table 2). Related direct ITC titrations (Supporting Information File 1, Figures S20–S29) were performed at a fixed concentration of Pr[6]AS (10 μM) with the remainder of the guest panel (Figure 3) and the thermodynamic parameters are reported in Table 2. Two of the primary ammonium ion guests (**3p**, (PXDA) and **5p**, (CHDA)) and the quaternary monoammonium guest (**1**, NMe_4) did not evolve sufficient heat when a Pr[6]AS concentration of 10 μM in the ITC cell was used due to low K_a values and/or low ΔH values. We avoided working at higher Pr[6]AS concentrations due to the potential differential impact of ion pairing as the concentration of the host is raised [59]. However, the

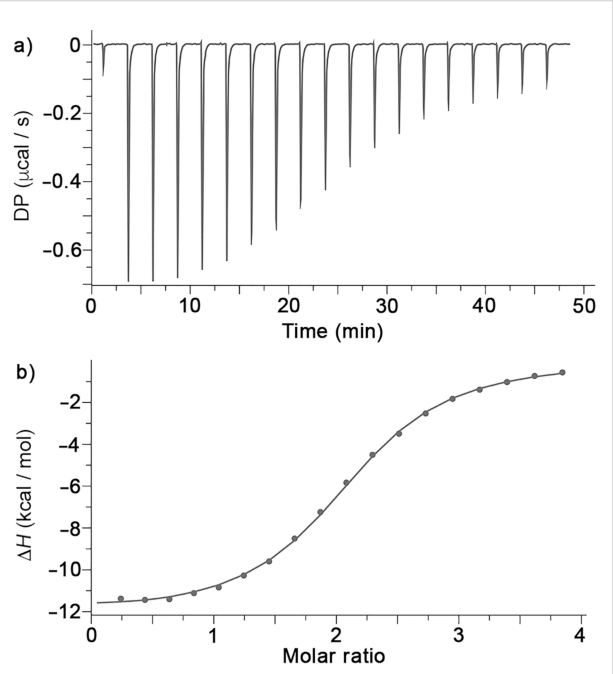


Figure 5: a) Plot of DP versus time from the titration of a mixture of Pr[6]AS (10 μM) in the cell with **6q** (200 μM) from the syringe. b) Plot of ΔH versus **6q**:Pr[6]AS molar ratio. The solid line represents the best fit of the data to a sequential binding model implemented in the PEAQ-ITC data analysis software with $K_{a1} = (1.28 \pm 0.11) \times 10^6$ M^{-1} and $\Delta H_1 = -12.33 \pm 1.15$ kcal mol^{-1} and $K_{a2} = (6.48 \pm 0.31) \times 10^5$ M^{-1} and $\Delta H_2 = -12.63 \pm 1.42$ kcal mol^{-1}.

^{1}H NMR spectra for mixtures of Pr[6]AS and either **3p** (PXDA), **5p** (CHDA), or **1** (NMe_4) (Supporting Information File 1, Figures S7, S8, and S10) show broadening and upfield shifting of guest resonances indicating that binding does occur.

Discussion of trends in the thermodynamic parameters

Table 2 shows that Pr[6]AS exclusively forms ternary Pr[6]AS·guest$_2$ complexes. The K_a values for the stronger binding event, presumably within the cavity of Pr[6]AS range from 3.58×10^5 M^{-1} for **2p** (C6DA) up to 4.48×10^7 M^{-1} for **4** (MV). This binding event is driven by favorable enthalpic changes with K_a values ranging from −4.05 kcal mol^{-1} (for **2p** (C6DA)) to −15.03 kcal mol^{-1} for **4** (MV). The second binding events are only slightly weaker (maximum of 29-fold for **4**) and are also driven by favorable enthalpic changes (ΔH from −7.56 to −14.23 kcal mol^{-1}). These favorable enthalpic changes suggest that the binding processes are driven by the non-classical hydrophobic effect [60,61] involving the release of encapsulated water molecules as has been established previously for a variety of macrocycles including prismarenes [56,62,63]. Overall, Pr[6]AS displays low levels of selectivity between the different quaternary ammonium ion guests as is highlighted by the composite binding parameter β ($K_{a1} \times K_{a2}$, units M^{-2}) given in Table 2. Previous studies of sulfated pillararenes and Pr[5]AS showed high levels of selectivity for quaternary diammonium over primary diammonium ions [53]. In contrast no clear trends are seen in the K_{a1} values for Pr[6]AS with **2p** (C6DA), **2s**

Table 2: Binding constants (K_a, M^{-1}) and thermodynamic parameter (ΔH, kcal mol^{-1}) for the various hosts and guests.

	Pr[6]AS K_{a1} (M^{-1}); ΔH_1 (kcal mol^{-1}) K_{a2} (M^{-1}); ΔH_2 (kcal mol^{-1}) β (M^{-2}); $\Delta H_1 + \Delta H_2$ (kcal mol^{-1})[b]	**Pr[5]AS** [53] K_{a1} (M^{-1}); ΔH_1 (kcal mol^{-1})	**P[6]AS** [53] K_{a1} (M^{-1}); ΔH_1 (kcal mol^{-1})
1, (NMe_4)	i.h.e.[c]	$(7.88 \pm 0.09) \times 10^5$; −1.60 ± 0.04	$(7.73 \pm 0.19) \times 10^5$; −6.95 ± 0.03
2p, C6DA	$(3.58 \pm 0.55) \times 10^5$; −4.05 ± 0.83 $(4.00 \pm 1.17) \times 10^4$; −9.62 ± 1.80 $(1.43 \pm 0.47) \times 10^{10}$; −13.67 ± 1.98	$(3.91 \pm 0.31) \times 10^7$; −2.83 ± 0.04	$(3.23 \pm 0.21) \times 10^8$; −9.38 ± 0.03
2s, Me_2C6DA	$(1.59 \pm 0.02) \times 10^6$; −7.35 ± 0.09 $(8.27 \pm 0.23) \times 10^4$; −14.23 ± 0.33 $(1.31 \pm 0.04) \times 10^{11}$; −21.58 ± 0.34	$(8.61 \pm 0.70) \times 10^8$; −10.38 ± 0.10	$(3.78 \pm 0.10) \times 10^9$; −12.10 ± 0.02
2t, Me_4C6DA	$(8.45 \pm 1.00) \times 10^5$; −9.35 ± 1.11 $(3.40 \pm 0.18) \times 10^5$; −12.37 ± 1.35 $(2.87 \pm 0.37) \times 10^{11}$; −21.72 ± 1.75	$(1.39 \pm 0.11) \times 10^9$; −5.29 ± 0.06	$(4.870 \pm 0.001) \times 10^{10}$; −14.47 ± 0.03
2q, Me_6C6DA	$(6.42 \pm 0.37) \times 10^5$; −10.57 ± 0.83 $(9.49 \pm 0.23) \times 10^5$; −11.47 ± 1.04 $(6.09 \pm 0.38) \times 10^{11}$; −22.14 ± 1.33	$(5.29 \pm 0.62) \times 10^9$; −4.72 ± 0.06	$(2.97 \pm 0.04) \times 10^{11}$; −16.41 ± 0.03
3p, PXDA	i.h.e.[c]	$(8.40 \pm 0.47) \times 10^5$; 0.52 ± 0.07	$(3.09 \pm 0.11) \times 10^7$; −7.42 ± 0.02
3q, Me_6PXDA	$(1.15 \pm 0.17) \times 10^6$; −5.78 ± 0.83 $(2.00 \pm 0.28) \times 10^5$; −8.49 ± 0.63 $(2.30 \pm 0.47) \times 10^{11}$; −14.27 ± 1.04	$(1.92 \pm 0.22) \times 10^9$; −10.04 ± 0.07	$(1.68 \pm 0.01) \times 10^{11}$; −14.30 ± 0.02
4, MV	$(4.48 \pm 0.04) \times 10^7$; −15.03 ± 0.08 $(1.55 \pm 0.02) \times 10^6$; −13.77 ± 0.09 $(6.94 \pm 0.12) \times 10^{13}$; −28.80 ± 0.12	$(8.61 \pm 0.70) \times 10^8$; −10.38 ± 0.10	$(1.92 \pm 0.03) \times 10^{10}$; −13.17 ± 0.02
5p, CHDA	i.h.e.[c]	$(8.04 \pm 0.64) \times 10^5$; −5.13 ± 0.05	$(3.38 \pm 0.22) \times 10^7$; −6.01 ± 0.02
5q, Me_6CHDA	$(1.41 \pm 0.03) \times 10^6$; −6.36 ± 0.05 $(2.57 \pm 0.04) \times 10^5$; −7.56 ± 0.22 $(3.62 \pm 0.08) \times 10^{11}$; −13.92 ± 0.23	$(4.13 \pm 0.45) \times 10^9$; −6.33 ± 0.05	$(5.89 \pm 0.02) \times 10^{10}$; −12.33 ± 0.01
6s, Bipip	$(1.11 \pm 0.01) \times 10^6$; −5.23 ± 0.02 $(2.09 \pm 0.02) \times 10^5$; −7.64 ± 0.14 $(2.31 \pm 0.03) \times 10^{11}$; −12.87 ± 0.14	$(7.32 \pm 0.78) \times 10^9$; −8.22 ± 0.06	$(1.46 \pm 0.07) \times 10^{10}$; −10.33 ± 0.03
6q, Me_4Bipip	$(1.28 \pm 0.11) \times 10^6$; −12.33 ± 1.15 $(6.48 \pm 0.31) \times 10^5$; −12.63 ± 1.42 $(8.29 \pm 0.82) \times 10^{11}$; −24.96 ± 1.83	$(1.51 \pm 0.10) \times 10^{12}$; −13.75 ± 0.21	$(9.17 \pm 0.28) \times 10^{11}$; −14.63 ± 0.07
7, PPCP	$(1.02 \pm 0.08) \times 10^6$; −9.08 ± 0.82 $(1.04 \pm 0.13) \times 10^5$; −15.77 ± 0.69 $(1.06 \pm 0.16) \times 10^{11}$; −24.85 ± 1.07	–[d]	–[d]

[a]Conditions: PBS buffer, pH 7.4, 298 K; [b]β is the composite binding parameter ($K_{a1} \times K_{a2}$, units M^{-2}); [c]i.h.e.: insufficient heat evolved at [Pr[6]AS] = 10 μM; [d]not reported/determined.

(Me_2C6DA), **2t** (Me_4C6DA), and **2q** (Me_6C6DA), although a gentle 43-fold increase in the composite β-values from **2p** (C6DA) to **2q** (Me_6C6DA) is observed (Table 2). Similarly, the β-value for **6q** (Me_4Bipip) is 3.6-fold larger than for **6s** (Bipip). In contrast, the ITC and ^{1}H NMR data show that the quaternary diammonium ions **3q** (Me_6PXDA) and **5q** (Me_6CHDA) bind substantially stronger than their primary diammonium ion analogues **3p** (PXDA) and **5p** (CHDA) as has previously been observed for Pr[5]AS [53]. The thermodynamic data in Table 2 also allows a comparison between Pr[6]AS and the previously reported sulfated hosts Pr[5]AS and P[6]AS [38,53]. Quite clearly, the K_{a1} values increase as the host is changed from Pr[6]AS to Pr[5]AS to P[6]AS which likely reflects: a) a better host:guest size match with this panel of guests, b) the presence of residual water molecules within the binary Pr[6]AS·guest complexes (vide infra), and c) the lower net charge of Pr[5]AS (−10 versus −12) compared to P[6]AS. In this regard, it is noteworthy that **6q** binds slightly tighter to Pr[5]AS than P[6]AS despite its lower charge.

Molecular dynamics simulations of Me_4Bipip (**6q**) binding to Pr[6]AS

The ITC results described above (Figure 5, Table 2) clearly establish that Pr[6]AS forms ternary Pr[6]AS·guest$_2$ complexes. However, the broadening observed in the ^{1}H NMR spectra of 1:1 and 1:2 mixtures of Pr[6]AS and guests (Figure 4 and Supporting Information File 1, Figures S7–S19) do not allow us to elucidate the geometry of the Pr[6]AS·guest$_2$ complexes (Figure 1b–e). Accordingly, we performed molecular dynamics simulations of the interaction of **6q** with Pr[6]AS. We simulated three systems in explicit TIP3P water [64] with 137 mM NaCl [65] to match the experimental ionic strength: 1) uncomplexed Pr[6]AS (50 ns), 2) Pr[6]AS·**6q** (1:1, 500 ns), and 3) Pr[6]AS·**6q$_2$** (1:2, 500 ns). We parametrized both host and guest with the OpenFF Sage 2.3.0 force field [66,67], using NAGL machine-learned AM1-BCC [68] charges for Pr[6]AS and AM1-BCC charges [69,70] for **6q**, and ran unbiased NPT production in OpenMM [71] at 300 K. Full simulation and analysis protocols are given in Supporting Information File 1. The position and orientation of **6q**, Pr[6]AS eccentricity, intersulfate distances, cavity hydration, and cation–water–sulfate bridges were computed with MDTraj [72] in a Pr[6]AS body frame defined independently for each frame. The body-frame axis was defined as the normal to the mean plane of the macrocycle. Guest positions were calculated by projecting the guest center of mass, relative to the host center of mass, onto this axis (z) and the perpendicular plane (r). The simulation involving the Pr[6]AS and **6q** at a 1:2 ratio was simulated from three different starting configurations: a) two molecules of **6q** at the edges of the simulation box, b) one molecule of **6q** inside Pr[6]AS and one bound at the sulfated portal (Figure 1c, Supporting Information File 1, Figure S31), and c) two molecules of **6q** inside Pr[6]AS (Figure 1b). Throughout these simulations, the macrocyclic scaffold maintained a radius of gyration 7.36–7.37 Å. This metric indicates that the host does not undergo large-scale collapse or expansion during the simulations while still sampling conformational changes in the macrocycle and sulfate groups.

Geometrical features of uncomplexed Pr[6]AS and the Pr[6]AS·**6q** and Pr[6]AS·**6q$_2$** complexes

Figure 6a shows a snapshot from the MD simulation of uncomplexed Pr[6]AS. Rather than assuming an idealized regular hexagonal geometry, Pr[6]AS assumes the more rectangular structure shown in Figure 6a. The longest distance between the opposing S-atoms amounts to 19.2 ± 0.4 Å. In the Pr[6]AS·**6q** complex (Figure 6b), **6q** binds along the cavity axis of Pr[6]AS: its center of mass sits close to the center of the host ($|z|$ = 1.68 ± 0.04 Å, r = 1.26 ± 0.02 Å) and its N–N axis is tilted 35.1 ± 0.7° from the macrocycle normal. Here z and r measure displacement along and perpendicular to the macrocycle normal, both relative to the center of mass of Pr[6]AS, and the tilt is the angle between that normal and the N–N axis of **6q**. One of the quaternary N-atoms of **6q** is located near three sulfates where it engages in NC–H···O interactions. Conversely, the other quaternary N-atom is located inside the cavity of Pr[6]AS where it engages in quaternary ammonium cation–π interactions with one of the naphthalene walls of Pr[6]AS. Figure 6c shows a snapshot (at 250 ns) from the MD simulation of Pr[6]AS·**6q$_2$**. Additional snapshots at t = 0, 16, 50, and 500 ns are shown in Supporting Information File 1, Figure S32. In the MD trajectory, the Pr[6]AS (−12) host binds the **6q** guests to its convex equatorial region followed by one **6q** entering the cavity at t = 16 ns; this guest remains bound for the remaining 484 ns of the simulation. In the 250 ns snapshot, one **6q** guest is bound inside the cavity of Pr[6]AS with a geometry that is quite similar to the 1:1 Pr[6]AS·**6q** complex (Figure 6b). The second **6q** molecule is located outside the cavity along the equatorial region of Pr[6]AS where it interacts with one naphthalene wall and two sulfate substituents; the overall geometry resembles that depicted in Figure 1e. At other timepoints in the simulation (16 and 50 ns) the second **6q** guest binds to the exterior naphthalene wall with the alternate axial-type geometry depicted in Figure 1d (Supporting Information File 1, Figure S32b,c). In this geometry, the **6q** guest interacts with three sulfate substituents. The **6q** guest binding at the equatorial region of Pr[6]AS is dynamic and visits ≈5–8 of the 12 sulfates and exchanges among them on the ≈100 ns timescale. The cavity guest is dynamic in a different sense. It does not leave the cavity over 484 ns, but the integrated autocorrelation time of its tilt angle is 5.3–8.9 ns, so it reorients within the cavity many times over each 500 ns trajectory.

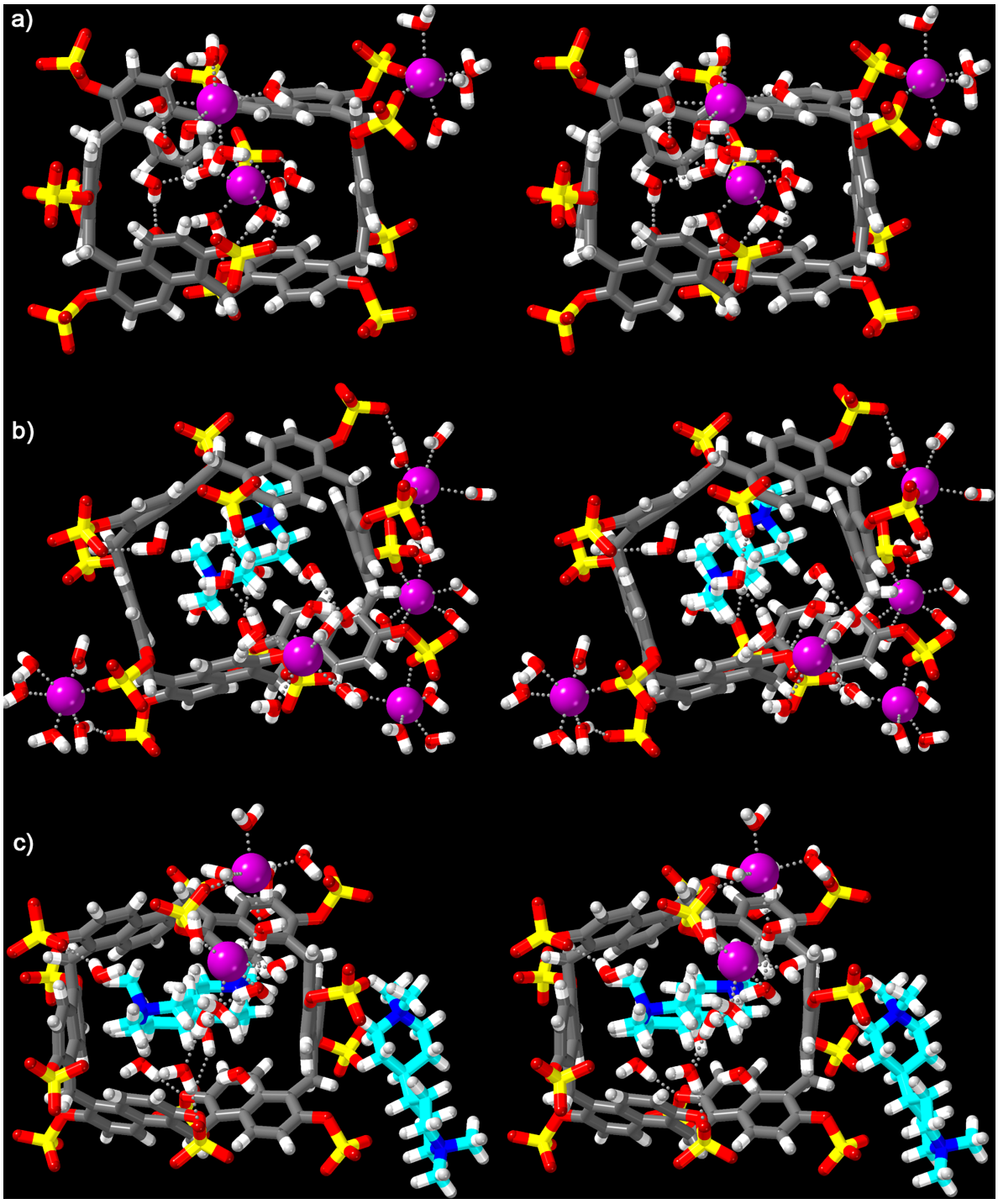


Figure 6: Cross-eyed stereoviews of the most representative solvation clusters from the MD simulations of: a) Pr[6]AS, b) Pr[6]AS·**6q**, and c) Pr[6]AS·**6q**$_2$. First-shell H_2O molecules and inner-sphere Na^+ ions (d(Na^+···O) < 3.15 Å) are shown; bulk H_2O, Cl^-, and remaining Na^+ are omitted for clarity. Color code: C atoms of Pr[6]AS, gray; C atoms of **6q**, aqua; H, white; N, blue; O, red; S, yellow; Na^+, purple; Na···O and HOH···O, gray dotted lines.

In none of the MD simulations were any Pr[6]AS·**6q**$_2$ complexes observed that possessed geometries of the type shown in Figure 1b. To further verify whether such a geometry might be possible, we deliberately forced two guests into the host cavity via docking and then minimized energy using three restraint protocols. Unrestrained minimization expelled both guests through opposite portals. With a flat-bottom restraint confining each guest's center of mass to within 4 Å of the host center,

minimization drove both guests to the cavity edges rather than to a deep-cavity minimum. With harmonic position restraints on all guest heavy atoms, which hold the docked geometry rigid, minimization converged to a strongly positive potential energy of $+4 \times 10^4$ kJ/mol, and NVT dynamics started from that structure produced NaN immediately. The force field therefore admits no local minimum with both **6q** (Me_4Bipip) inside the cavity. In fact, when a Pr[6]AS·$\mathbf{6q}_2$ complex with an initial geometry similar to Figure 1c was used for the MD simulation, the complex transformed into that depicted in cartoon form in Figure 1e (e.g., Figure 6c).

Water-mediated interactions and cavity desolvation

We used the MD simulations discussed above to quantify the water-mediated interactions between Pr[6]AS and **6q**. Each cavity bound **6q** interacts with roughly three first-shell H_2O molecules via N^+CH_2–H···OH_2 interactions; these three H_2O molecules also form H-bonds to a terminal sulfate oxygen atom (Figure 6b). The number of first-shell H_2O molecules is the same in both Pr[6]AS·**6q** and Pr[6]AS·$\mathbf{6q}_2$ complexes. A histogram of the number of H_2O molecules located in the cavity of Pr[6]AS, Pr[6]AS·**6q**, and Pr[6]AS·$\mathbf{6q}_2$ is given in Supporting Information File 1 (Figure S33). Uncomplexed Pr[6]AS holds 7.6 ± 1.9 water molecules and one Na^+ ion in its cavity, whereas Pr[6]AS·**6q** holds 3.1 ± 1.1 and the two Pr[6]AS·$\mathbf{6q}_2$ simulations each hold 2.9 ± 1.1. Thus, binding of **6q** displaces approximately five molecules of water and one Na^+ ion from the cavity of Pr[6]AS. Mapping the water density around Pr[6]AS·$\mathbf{6q}_2$ in a reference frame fixed to the host (Supporting Information File 1, Figure S34) shows where that water is lost and where it is retained. Binding of **6q** inside Pr[6]AS results in cavity desolvation (decreases to ≈10% of bulk water density) whereas the twelve sulfate groups retain discrete bridging hydration shells at 2–3 times bulk water density. Overall, **6q** binding desolvates the hydrophobic cavity (loss of ≈60% of water) but not the anionic sulfated portal (loss of only ≈7% of water) because **6q** inserts into a preexisting sulfate hydration shell rather than displacing it.

Previously, the deficiency of H-bonds of water molecules inside the cavity of CB[*n*] hosts was shown to play an important role in their ultratight binding [62,63,73]. Uncomplexed Pr[6]AS binds 7.6 ± 1.9 water molecules in its cavity, and in 92% of the frames a Na^+ ion is also present, coordinated by about four of these waters. Using the criteria of Biedermann, Nau, and Schneider [63] (donor–acceptor ≤ 3.5 Å, D–H···A ≥ 130°) we find that the remaining cavity waters form approximately 3.1 H-bonds which is slightly less than the bulk water (3.66 H-bonds) in our simulations. In 8% of the frames (42 events) the cavity of Pr[6]AS is occupied by 9.5 ± 0.1 waters which form 2.95 ± 0.1 H-bonds (Supporting Information File 1, Figure S36) which results in a deficiency of H-bonds ($Z = 9.5 \times (3.62 - 2.95) = 6.4$ H-bonds). This Z-value lies between those previously calculated for CB[6] (3.3 cavity waters, 1.71 H-bonds, $Z = 6.3$) and CB[8] (13.1 cavity waters; 3.06 H-bonds; $Z = 7.3$) both of which are ultratight binding hosts [63]. However, Setiadi, Biedermann, Nau, and Gilson recently showed that structural measurements of cavity water, such as water density, do not necessarily correlate with its energetics [73]. Our simulations, therefore, cannot establish whether the waters inside the cavity water of Pr[6]AS are high-energy. The MD simulations do show that when no Na^+ is present, the cavity waters form fewer hydrogen bonds than bulk water and releasing such water could favor binding. While expulsion of under-coordinated cavity water is consistent with the enthalpy-driven bimolecular association to give Pr[6]AS·**6q** ($\Delta H_1 = -12.3$ kcal/mol, $-T\Delta S \approx +4$ kcal/mol), our simulations cannot determine what fraction of the measured binding enthalpy comes from release of the cavity Na^+ from the cavity versus release of cavity water.

Counterion release and sodium coordination

Binding displaces counterions which have ordered around the host, as well as water. Pr[6]AS has a charge of −12 and carries a sodium atmosphere comprising ≈3.5 inner-sphere Na^+ contact-ion pairs at the sulfated portal and roughly one Na^+ located in the center of the cavity of Pr[6]AS (Figure 6a). Complexation of dicationic **6q** by Pr[6]AS results in the translocation of the cavity Na^+ ion to the sulfated portal (Figure 6c). The average number of inner-sphere Na^+ ions at the sulfated portal decreases to 2.3 in Pr[6]AS·**6q** and to 1.9 and 1.5 in the two Pr[6]AS·$6q_2$ simulations (Supporting Information File 1, Figure S35a). The Na^+···sulfate contact distance is ≈2.4 Å (Supporting Information File 1, Figure S35b) as expected. Overall, **6q** binding is an exchange process that involves expulsion of cavity Na^+ and some cavity water. Chloride counteranions are not observed interacting with the cavity bound **6q** guest.

Host conformational analysis

To gain insight into the conformational flexibility and structural characteristics of the host, we analyzed two key structural parameters: 1) the S···S distances between the sulfate groups of Pr[6]AS, and 2) the distortion away from circularity of both the sulfate groups and the CH_2 groups of the macrocyclic core as measured by the eccentricity parameter (e). We define two S···S distances: d_{adj} measures the separation between sulfate groups on adjacent naphthalene rings on the same portal (12 such pairs), and d_{opp} measures the distance between sulfate groups of the same naphthalene ring located on opposite portals (6 pairs). The d_{adj} distance averages 8.20 ± 0.03 Å for Pr[6]AS and decreases to 7.86 ± 0.03 Å upon binding **6q** whereas the d_{opp} distance is invariant at 9.50 ± 0.03 Å (Figure 7a). The quoted error is the standard error across the complexes; the frame-to-

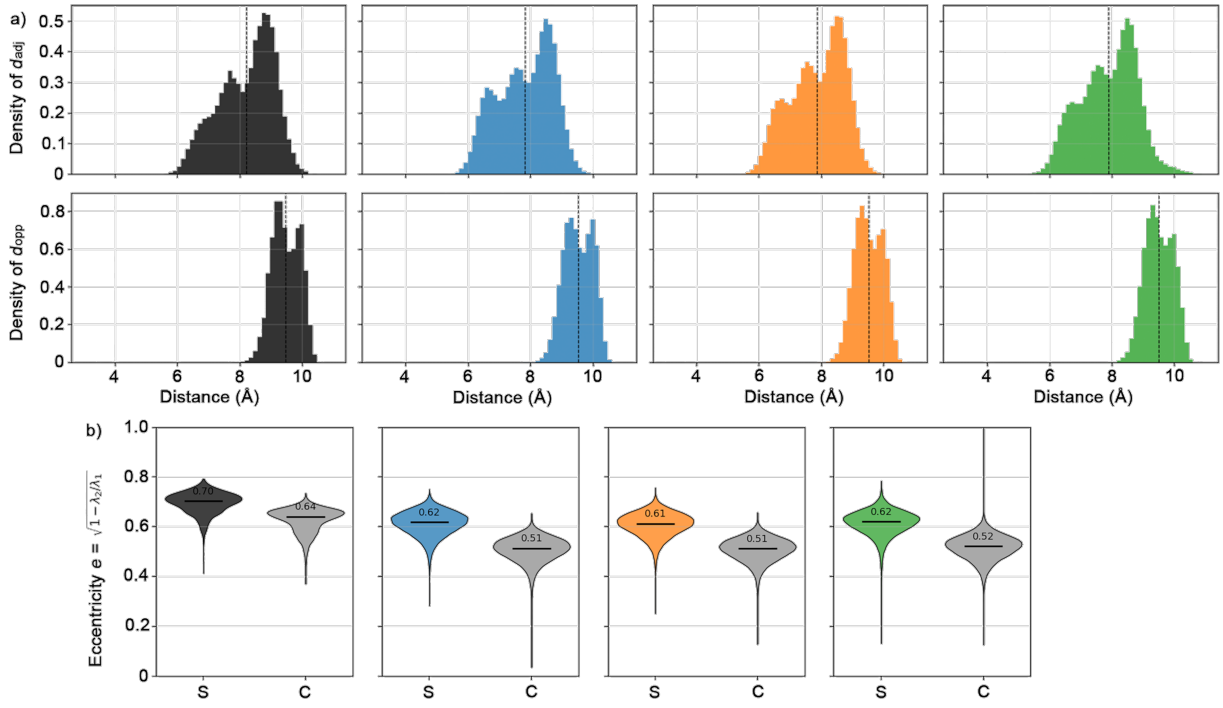


Figure 7: Conformation of Pr[6]AS upon complexation of **6q**. a) Distributions of the inter-sulfate distances d_{adj} (top) and d_{opp} (bottom); dashed vertical lines mark the mean of each distribution. b) Violin plots of the eccentricity, $e = \sqrt{(1 - \lambda_2/\lambda_1)}$, of the sulfate S-atoms (S, ionic) and the bridging CH_2 C-atoms (C, macrocyclic core); horizontal bars and inset values give the means. Columns, left to right: Pr[6]AS (black), Pr[6]AS·**6q** (blue), Pr[6]AS·**6q**$_2$ (orange, starting from the geometry of Figure 1c), and Pr[6]AS·**6q**$_2$ (green, starting from uncomplexed **6q**).

frame standard deviation of d_{adj} is 0.9 Å. The 12 sulfate groups of uncomplexed Pr[6]AS do not sit at a common distance from the macrocycle axis. They occupy three shells at 4.1, 7.5, and 9.4 Å. Upon binding **6q**, the four sulfates of the innermost shell move outward by 0.6 to 1.7 Å and the remaining eight move inward by 0.5 Å or less. The average sulfate distance from the axis is 7.01 Å for uncomplexed Pr[6]AS and 7.15 Å for the complexes, and the root-mean-square displacement over the 12 sulfates is 0.7 Å. The decrease of d_{adj}, therefore, reflects a rearrangement of the sulfate groups and not a compression of the host.

Finally, we examined the eccentricity of both the sulfate groups and the CH_2 carbon atoms of the macrocyclic core to quantify the overall structural asymmetry and the degree of deformation of Pr[6]AS upon complexation (Figure 7b). Eccentricity measures how much an ellipse deviates from being a perfect circle, with 0 being circular and 1 being the extreme where an ellipse opens into a parabola. Here, the ionic-group eccentricity falls from e(sulfates) = 0.70 for uncomplexed Pr[6]AS to 0.62 upon complexation to form Pr[6]AS·**6q**. In contrast to the sulfated pillar[5]arenes whose macrocyclic core was found to retain its circular shape [40], the bridging CH_2 groups of Pr[6]AS are not rigid. The CH_2 group eccentricity of Pr[6]AS drops from $e(CH_2)$ = 0.62 for Pr[6]AS to 0.51 for Pr[6]AS·**6q** which amounts to a shift of 19 standard errors further supporting the notion that the macrocyclic backbone of Pr[6]AS tightens upon **6q** complexation. The simulations of the Pr[6]AS·**6q** and Pr[6]AS·**6q**$_2$ all converge to the same geometry (Δ ≤1 SEM on each metric) which indicates that the second guest binding does not further distort or symmetrize Pr[6]AS host. The first molecule of **6q** induces all the structural changes in the same way that the first **6q** binding event triggers desolvation. Overall, **6q** binding changes the conformation of Pr[6]AS without changing its size measured in several different ways. That is, the radius of gyration (7.37 Å), the average sulfate distance from the axis, and the d_{opp} distance are all the same (within error) in the uncomplexed versus the bound host. The size-preserving conformational changes are thus of two kinds. First, the sulfate groups rearrange: in uncomplexed Pr[6]AS four of the 12 sulfates sit 4.1 Å from the axis and partially block the cavity, and **6q** displaces these four outward by 0.6 to 1.7 Å while the other eight move inward, which leaves the 12 sulfates at more similar distances from the axis. Second, the macrocyclic backbone itself changes shape, as shown by the drop in $e(CH_2)$ from 0.62 to 0.51. Both the sulfate groups and the CH_2 core are more circular in the complex than in the free host. Pr[6]AS remains flexible in both states: d_{adj} fluctuates by

±0.9 Å and *e*(sulfates) by ±0.04 over the course of the simulations, so binding shifts the average conformation of Pr[6]AS rather than rigidifying it.

Conclusion

In summary, we report the synthesis of Pr[6]AS which displays good water solubility (≥30 mM) and low self-association according to ^{1}H NMR dilution and variable-temperature experiments. ITC experiments established that Pr[6]AS forms ternary host–guest complexes with β-values ($K_{a1} \times K_{a2}$) values up to 6.84×10^{13} M^{-2} in PBS. Quaternary ammonium ion guests bind more tightly than the analogous primary ammonium ion form. ^{1}H NMR spectroscopy of the host–guest complexes of Pr[6]AS show upfield shifting upon complexation, but dramatic broadening prevents structural elucidation. Molecular dynamics simulations showed that Pr[6]AS binds one **6q** in its cavity whereas the second guest binds on the convex face in close proximity to the externally directed sulfate substituents. The formation of 1:1 and 1:2 Pr[6]AS·**6q** complexes results in the expulsion of the cavity-bound Na^+ ion and much of the cavity waters. In conclusion, the work shows that ionic sulfate groups are not merely spectators around a hydrophobic cavity, but rather active participants that shape the exterior of the host and promote ternary complex formation.

Supporting Information

The electronic data that support this publication can be freely downloaded from the Digital Repository at the University of Maryland (https://drum.lib.umd.edu/home) via the following doi:10.13016/s4v4-dkcq. The electronic data from the molecular dynamics simulations can be accessed at the following doi:10.5281/zenodo.23380489.

Supporting Information File 1

Experimental materials, methods, and procedures, copies of ^{1}H, ^{13}C NMR, and DOSY spectra, ITC thermograms and coordinates from molecular modelling.
[https://www.beilstein-journals.org/bjoc/content/supplementary/1860-5397-22-132-S1.pdf]

Acknowledgements

We thank Dr. Gurpreet Kaur for providing a sample of **7** (PPCP).

Funding

L.I. and E.B.B. thank the National Science Foundation (CHE-2105857) for financial support. S.A. and D.L.M. thank the National Institutes of Health (R35GM148236) for financial support.

Conflict of Interest

L.I. is co-founder and holds equity in Reversal Therapeutics (College Park, Maryland, United States) and holds equity in Clear Scientific (Cambridge, Massachusetts, United States).

ORCID® iDs

Steven Ayoub - https://orcid.org/0000-0002-2099-4669
David L. Mobley - https://orcid.org/0000-0002-1083-5533
Lyle Isaacs - https://orcid.org/0000-0002-4079-332X

Data Availability Statement

Data generated and analyzed during this study is openly available from the Digital Repository at the University of Maryland at https://doi.org/ https://doi.org/10.13016/s4v4-dkcq and at Zenodo: https://doi.org/10.5281/zenodo.23380489.

Preprint

A non-peer-reviewed version of this article has been previously published as a preprint: doi:10.26434/chemrxiv.15007937/v1

References

1. You, L.; Zha, D.; Anslyn, E. V. *Chem. Rev.* **2015,** *115,* 7840–7892. doi:10.1021/cr5005524
2. Dempsey, J. M.; Zhai, C.; McGarraugh, H. H.; Schreiber, C. L.; Stoffel, S. E.; Johnson, A.; Smith, B. D. *Chem. Commun.* **2019,** *55,* 12793–12796. doi:10.1039/c9cc05244e
3. Zimmerman, S. C.; Kwan, W.-S. *Angew. Chem., Int. Ed. Engl.* **1995,** *34,* 2404–2406. doi:10.1002/anie.199524041
4. Ligthart, G. B. W. L.; Ohkawa, H.; Sijbesma, R. P.; Meijer, E. W. *J. Am. Chem. Soc.* **2005,** *127,* 810–811. doi:10.1021/ja043555t
5. Webber, M. J.; Langer, R. *Chem. Soc. Rev.* **2017,** *46,* 6600–6620. doi:10.1039/c7cs00391a
6. Finnegan, T. J.; Gunawardana, V. W. L.; Badjić, J. D. *Chem. – Eur. J.* **2021,** *27,* 13280–13305. doi:10.1002/chem.202101532
7. Diederich, F. *Angew. Chem., Int. Ed. Engl.* **1988,** *27,* 362–386. doi:10.1002/anie.198803621
8. Rekharsky, M. V.; Inoue, Y. *Chem. Rev.* **1998,** *98,* 1875–1918. doi:10.1021/cr970015o
9. Gutsche, C. D. *Acc. Chem. Res.* **1983,** *16,* 161–170. doi:10.1021/ar00089a003
10. Pedersen, C. J. *Angew. Chem., Int. Ed. Engl.* **1988,** *27,* 1021–1027. doi:10.1002/anie.198810211
11. Jordan, J. H.; Gibb, B. C. *Chem. Soc. Rev.* **2015,** *44,* 547–585. doi:10.1039/c4cs00191e
12. Domoto, Y.; Fujita, M. *Coord. Chem. Rev.* **2022,** *466,* 214605. doi:10.1016/j.ccr.2022.214605
13. Kraft, A.; Schmidt, C. R.; Akakpo, C.; Biedermann, F.; Webber, M. J.; Isaacs, L. *Nat. Rev. Methods Primers* **2026,** *6,* 40. doi:10.1038/s43586-026-00495-2
14. Ogoshi, T.; Yamagishi, T.-a.; Nakamoto, Y. *Chem. Rev.* **2016,** *116,* 7937–8002. doi:10.1021/acs.chemrev.5b00765
15. Khalil-Cruz, L. E.; Liu, P.; Huang, F.; Khashab, N. M. *ACS Appl. Mater. Interfaces* **2021,** *13,* 31337–31354. doi:10.1021/acsami.1c05798

16. Ahn, Y.; Jang, Y.; Selvapalam, N.; Yun, G.; Kim, K. *Angew. Chem., Int. Ed.* **2013,** *52,* 3140–3144. doi:10.1002/anie.201209382
17. Park, K. M.; Murray, J.; Kim, K. *Acc. Chem. Res.* **2017,** *50,* 644–646. doi:10.1021/acs.accounts.6b00645
18. Ganapati, S.; Grabitz, S. D.; Murkli, S.; Scheffenbichler, F.; Rudolph, M. I.; Zavalij, P. Y.; Eikermann, M.; Isaacs, L. *ChemBioChem* **2017,** *18,* 1583–1588. doi:10.1002/cbic.201700289
19. Liu, W.; Samanta, S. K.; Smith, B. D.; Isaacs, L. *Chem. Soc. Rev.* **2017,** *46,* 2391–2403. doi:10.1039/c7cs00011a
20. Chen, F.-Y.; Fu, R.; Gong, Z.; Li, C.; Guo, D.-S.; Cai, K. *Angew. Chem., Int. Ed.* **2025,** *64,* e202500916. doi:10.1002/anie.202500916
21. Stella, V. J.; Rajewski, R. A. *Pharm. Res.* **1997,** *14,* 556–567. doi:10.1023/a:1012136608249
22. Fu, R.; Chen, F.-Y.; Dai, L.; Li, D.-Y.; Zhao, Q.-Y.; Guo, S.-D.; Song, Z.-H.; Jing, L.-B.; Wang, H.; Li, X.; Guo, D.-S.; Cai, K. *Nat. Commun.* **2025,** *16,* 9718. doi:10.1038/s41467-025-64739-7
23. Kiguchi, M.; Takahashi, T.; Takahashi, Y.; Yamauchi, Y.; Murase, T.; Fujita, M.; Tada, T.; Watanabe, S. *Angew. Chem., Int. Ed.* **2011,** *50,* 5708–5711. doi:10.1002/anie.201100431
24. Kim, J.; Jung, I.-S.; Kim, S.-Y.; Lee, E.; Kang, J.-K.; Sakamoto, S.; Yamaguchi, K.; Kim, K. *J. Am. Chem. Soc.* **2000,** *122,* 540–541. doi:10.1021/ja993376p
25. Ko, Y. H.; Kim, E.; Hwang, I.; Kim, K. *Chem. Commun.* **2007,** 1305–1315. doi:10.1039/b615103e
26. Rowland, M. J.; Parkins, C. C.; McAbee, J. H.; Kolb, A. K.; Hein, R.; Loh, X. J.; Watts, C.; Scherman, O. A. *Biomaterials* **2018,** *179,* 199–208. doi:10.1016/j.biomaterials.2018.05.054
27. Nguyen, H. D.; Dang, D. T.; van Dongen, J. L. J.; Brunsveld, L. *Angew. Chem.* **2010,** *122,* 907–910. doi:10.1002/ange.200904413
28. Rebek, J., Jr. *Acc. Chem. Res.* **2009,** *42,* 1660–1668. doi:10.1021/ar9001203
29. Harris, K.; Fujita, D.; Fujita, M. *Chem. Commun.* **2013,** *49,* 6703–6712. doi:10.1039/c3cc43191f
30. Ueda, Y.; Ito, H.; Fujita, D.; Fujita, M. *J. Am. Chem. Soc.* **2017,** *139,* 6090–6093. doi:10.1021/jacs.7b02745
31. Ashbridge, Z.; Reek, J. N. H. *Nat. Synth.* **2024,** *3,* 1197–1207. doi:10.1038/s44160-024-00606-5
32. Craescu, C. V.; Stahl, S.; Correia, T. L. F.; Bierschenk, S. M.; Settineri, N. S.; Bergman, R. G.; Raymond, K. N.; Toste, F. D. *J. Am. Chem. Soc.* **2025,** *147,* 32600–32609. doi:10.1021/jacs.5c07697
33. Murase, T.; Otsuka, K.; Fujita, M. *J. Am. Chem. Soc.* **2010,** *132,* 7864–7865. doi:10.1021/ja103109z
34. Fujita, M.; Oguro, D.; Miyazawa, M.; Oka, H.; Yamaguchi, K.; Ogura, K. *Nature* **1995,** *378,* 469–471. doi:10.1038/378469a0
35. Finnegan, T. J.; Mortensen, C.; Badjić, J. D. *Chem. Commun.* **2024,** *60,* 1936–1939. doi:10.1039/d3cc05485c
36. Karmakar, P.; Finnegan, T. J.; Rostam, D. C.; Taneja, S.; Uçar, S.; Hansen, A. L.; Moore, C. E.; Hadad, C. M.; Pratumyot, K.; Parquette, J. R.; Badjić, J. D. *Chem. Sci.* **2024,** *15,* 10155–10163. doi:10.1039/d3sc05627a
37. Yu, G.; Xue, M.; Zhang, Z.; Li, J.; Han, C.; Huang, F. *J. Am. Chem. Soc.* **2012,** *134,* 13248–13251. doi:10.1021/ja306399f
38. Xue, W.; Zavalij, P. Y.; Isaacs, L. *Angew. Chem., Int. Ed.* **2020,** *59,* 13313–13319. doi:10.1002/anie.202005902
39. King, D.; Wilson, C. R.; Herron, L.; Deng, C.-L.; Mehdi, S.; Tiwary, P.; Hof, F.; Isaacs, L. *Org. Biomol. Chem.* **2022,** *20,* 7429–7438. doi:10.1039/d2ob01487d
40. Goswami, A.; Çınaroğlu, S. S.; Singh, N.; Zavalij, P. Y.; Mobley, D. L.; Isaacs, L. *Chem. – Eur. J.* **2025,** *31,* e202404024. doi:10.1002/chem.202404024
41. Brockett, A. T.; Xue, W.; King, D.; Deng, C.-L.; Zhai, C.; Shuster, M.; Rastogi, S.; Briken, V.; Roesch, M. R.; Isaacs, L. *Chem* **2023,** *9,* 881–900. doi:10.1016/j.chempr.2022.11.019
42. Zhang, W.; Bazan-Bergamino, E. A.; Doan, A. P.; Zhang, X.; Isaacs, L. *Chem. Commun.* **2024,** *60,* 4350–4353. doi:10.1039/d4cc00772g
43. Chen, L.; Jiang, K.; Liu, Y.; Song, M.; Zhao, Y.; Tian, C.; Zhang, Y.; Zhang, Z.; Yu, X.; Xiao, J.; Chen, J.; Yong, Z.; Li, C.; Meng, Q. *SmartMat* **2025,** *6,* e70020. doi:10.1002/smm2.70020
44. Wang, R.; Fang, Z.; Li, S.; Zhang, Z.; Dong, M.; Chen, J.; Meng, Q.; Li, C. *Chem. Sci.* **2025,** *16,* 1321–1326. doi:10.1039/d4sc06859a
45. Zhao, Y.; Chen, L.; Chen, J.; Li, J.; Meng, Q.; Sue, A. C.-H.; Li, C. *Chem. Commun.* **2023,** *59,* 5858–5861. doi:10.1039/d3cc01405c
46. Ueno, M.; Sugiyama, H.; Li, F.; Nishimura, T.; Arakawa, H.; Chen, X.; Cheng, X.; Takeuchi, S.; Takeshita, Y.; Takamura, T.; Miyagi, S.; Toyama, T.; Soga, T.; Masuo, Y.; Kato, Y.; Nakamura, H.; Tsujiguchi, H.; Hara, A.; Tajima, A.; Noguchi-Shinohara, M.; Ono, K.; Kurayoshi, K.; Kobayashi, M.; Tadokoro, Y.; Kasahara, A.; Shoulkamy, M. I.; Maeda, K.; Ogoshi, T.; Hirao, A. *Anal. Chem. (Washington, DC, U. S.)* **2024,** *96,* 14499–14507. doi:10.1021/acs.analchem.4c02653
47. Prabodh, A.; Grimm, L. M.; Biswas, P. K.; Mahram, V.; Biedermann, F. *Chem. – Eur. J.* **2024,** *30,* e202401071. doi:10.1002/chem.202401071
48. Wang, R.; Li, W.-B.; Deng, J.-Y.; Han, H.; Chen, F.-Y.; Li, D.-Y.; Jing, L.-B.; Song, Z.; Fu, R.; Guo, D.-S.; Cai, K. *Angew. Chem., Int. Ed.* **2024,** *63,* e202317402. doi:10.1002/anie.202317402
49. Chen, L.; Jiang, K.; Pan, R.; Ye, J.; Chen, J.; Zhao, Y.; Qiu, T.; Su, P.; Zhang, D.; Ye, C.; Cai, W.; Xu, Z.; Miao, X. *RSC Adv.* **2026,** *16,* 38449–38454. doi:10.1039/d6ra02977a
50. Della Sala, P.; Del Regno, R.; Talotta, C.; Capobianco, A.; Hickey, N.; Geremia, S.; De Rosa, M.; Spinella, A.; Soriente, A.; Neri, P.; Gaeta, C. *J. Am. Chem. Soc.* **2020,** *142,* 1752–1756. doi:10.1021/jacs.9b12216
51. Del Regno, R.; Santonoceta, G. D. G.; Della Sala, P.; De Rosa, M.; Soriente, A.; Talotta, C.; Spinella, A.; Neri, P.; Sgarlata, C.; Gaeta, C. *Org. Lett.* **2022,** *24,* 2711–2715. doi:10.1021/acs.orglett.2c00819
52. Zhai, C.; Isaacs, L. *Chem. – Eur. J.* **2022,** *28,* e202201743. doi:10.1002/chem.202201743
53. Bazan-Bergamino, E. A.; Isaacs, L. *Chem. – Eur. J.* **2026,** *32,* e71201. doi:10.1002/chem.71201
54. Palmieri, A.; Della Sala, P.; Del Regno, R.; Di Filippo, N.; Iuliano, V.; Talotta, C.; De Rosa, M.; Aragoni, M. C.; Caltagirone, C.; Picci, G.; Zaleskaya-Hernik, M.; Santonoceta, G. D. G.; Sgarlata, C.; Gaeta, C. *Commun. Chem.* **2026,** *9,* 307. doi:10.1038/s42004-026-02090-8
55. Del Regno, R.; Campanile, G.; Neri, P.; Talotta, C.; Rescifina, A.; Sgarlata, C.; Santonoceta, G. D. G.; Gaeta, C.; De Rosa, M. *Chem. Sci.* **2025,** *16,* 18223–18232. doi:10.1039/d5sc03155a
56. Del Regno, R.; Della Sala, P.; Santonoceta, G. D. G.; Neri, P.; De Rosa, M.; Talotta, C.; Sgarlata, C.; De Simone, A.; Gaeta, C. *Chem. – Eur. J.* **2024,** *30,* e202401734. doi:10.1002/chem.202401734
57. Del Regno, R.; Della Sala, P.; Picariello, D.; Talotta, C.; Spinella, A.; Neri, P.; Gaeta, C. *Org. Lett.* **2021,** *23,* 8143–8146. doi:10.1021/acs.orglett.1c02800
58. Della Sala, P.; Del Regno, R.; Di Marino, L.; Calabrese, C.; Palo, C.; Talotta, C.; Geremia, S.; Hickey, N.; Capobianco, A.; Neri, P.; Gaeta, C. *Chem. Sci.* **2021,** *12,* 9952–9961. doi:10.1039/d1sc02199k
59. Gómez-Gonzáles, B.; Basílio, N.; Vaz, B.; Pérez-Lorenzo, M.; García-Río, L. *Angew. Chem., Int. Ed.* **2024,** *63,* e202317553. doi:10.1002/anie.202317553

60. Meyer, E. A.; Castellano, R. K.; Diederich, F. *Angew. Chem., Int. Ed.* **2003,** *42,* 1210–1250. doi:10.1002/anie.200390319
61. Persch, E.; Dumele, O.; Diederich, F. *Angew. Chem., Int. Ed.* **2015,** *54,* 3290–3327. doi:10.1002/anie.201408487
62. Biedermann, F.; Uzunova, V. D.; Scherman, O. A.; Nau, W. M.; De Simone, A. *J. Am. Chem. Soc.* **2012,** *134,* 15318–15323. doi:10.1021/ja303309e
63. Biedermann, F.; Nau, W. M.; Schneider, H.-J. *Angew. Chem., Int. Ed.* **2014,** *53,* 11158–11171. doi:10.1002/anie.201310958
64. Jorgensen, W. L.; Chandrasekhar, J.; Madura, J. D.; Impey, R. W.; Klein, M. L. *J. Chem. Phys.* **1983,** *79,* 926–935. doi:10.1063/1.445869
65. Joung, I. S.; Cheatham, T. E., III. *J. Phys. Chem. B* **2008,** *112,* 9020–9041. doi:10.1021/jp8001614
66. Mobley, D. L.; Bannan, C. C.; Rizzi, A.; Bayly, C. I.; Chodera, J. D.; Lim, V. T.; Lim, N. M.; Beauchamp, K. A.; Slochower, D. R.; Shirts, M. R.; Gilson, M. K.; Eastman, P. K. *J. Chem. Theory Comput.* **2018,** *14,* 6076–6092. doi:10.1021/acs.jctc.8b00640
67. Boothroyd, S.; Behera, P. K.; Madin, O. C.; Hahn, D. F.; Jang, H.; Gapsys, V.; Wagner, J. R.; Horton, J. T.; Dotson, D. L.; Thompson, M. W.; Maat, J.; Gokey, T.; Wang, L.-P.; Cole, D. J.; Gilson, M. K.; Chodera, J. D.; Bayly, C. I.; Shirts, M. R.; Mobley, D. L. *J. Chem. Theory Comput.* **2023,** *19,* 3251–3275. doi:10.1021/acs.jctc.3c00039
68. *OpenFF NAGL; model openff-gnn-am1bcc-1.0.0*; Neural Network Approach to Generate Atomic-Level charges; Open Force Field Initiative. https://docs.openforcefield.org/projects/nagl/ (accessed Aug 19, 2026).
69. Jakalian, A.; Bush, B. L.; Jack, D. B.; Bayly, C. I. *J. Comput. Chem.* **2000,** *21,* 132–146. doi:10.1002/(sici)1096-987x(20000130)21:2<132::aid-jcc5>3.0.co;2-p
70. Jakalian, A.; Jack, D. B.; Bayly, C. I. *J. Comput. Chem.* **2002,** *23,* 1623–1641. doi:10.1002/jcc.10128
71. Eastman, P.; Galvelis, R.; Peláez, R. P.; Abreu, C. R. A.; Farr, S. E.; Gallicchio, E.; Gorenko, A.; Henry, M. M.; Hu, F.; Huang, J.; Krämer, A.; Michel, J.; Mitchell, J. A.; Pande, V. S.; Rodrigues, J. P.; Rodriguez-Guerra, J.; Simmonett, A. C.; Singh, S.; Swails, J.; Turner, P.; Wang, Y.; Zhang, I.; Chodera, J. D.; De Fabritiis, G.; Markland, T. E. *J. Phys. Chem. B* **2024,** *128,* 109–116. doi:10.1021/acs.jpcb.3c06662
72. McGibbon, R. T.; Beauchamp, K. A.; Harrigan, M. P.; Klein, C.; Swails, J. M.; Hernández, C. X.; Schwantes, C. R.; Wang, L.-P.; Lane, T. J.; Pande, V. S. *Biophys. J.* **2015,** *109,* 1528–1532. doi:10.1016/j.bpj.2015.08.015
73. Setiadi, J.; Biedermann, F.; Nau, W. M.; Gilson, M. K. *Angew. Chem., Int. Ed.* **2025,** *64,* e202505713. doi:10.1002/anie.202505713

License and Terms

This is an open access article licensed under the terms of the Beilstein-Institut Open Access License Agreement (https://www.beilstein-journals.org/bjoc/terms), which is identical to the Creative Commons Attribution 4.0 International License (https://creativecommons.org/licenses/by/4.0). The reuse of material under this license requires that the author(s), source and license are credited. Third-party material in this article could be subject to other licenses (typically indicated in the credit line), and in this case, users are required to obtain permission from the license holder to reuse the material.

The definitive version of this article is the electronic one which can be found at:
https://doi.org/10.3762/bjoc.22.132